

Energetics and structural properties of three-dimensional bosonic clusters near threshold

G. J. Hanna and D. Blume¹

¹*Department of Physics and Astronomy, Washington State University, Pullman, Washington 99164-2814*

(Dated: June 30, 2018)

We treat three-dimensional bosonic clusters with up to $N = 40$ atoms, interacting additively through two-body Van der Waals potentials, in the near-threshold regime. Our study includes super-borromean systems with N atoms for which all subsystems are unbound. We determine the energetics and structural properties such as the expectation value of the interparticle distance as a function of the coupling strength. It has been shown that the coupling strength $g_*^{(N)}$, for which the N -body system becomes unbound, is bounded by the coupling constant $g_*^{(N-1)}$, for which the next smaller system with $N - 1$ atoms becomes unbound, i.e., $g_*^{(N)} \geq (N - 1)g_*^{(N-1)}/N$. By fitting our numerically determined ground state energies to a simple functional form with three fitting parameters, we determine the relationship between $g_*^{(N)}$ and $g_*^{(N-1)}$. Our trimer and tetramer energies fall on the so-called Tjon line, which has been studied in nuclear physics. We confirm the existence of generalized Tjon lines for larger clusters. Signatures of the universal behavior of weakly-bound three-dimensional clusters can possibly be observed in ultracold Bose gases.

PACS numbers:

I. INTRODUCTION

Weakly-bound few-body systems have been studied extensively by the atomic, nuclear and condensed matter physics community since the early days of quantum mechanics. Within the framework of non-relativistic quantum mechanics, the properties of a many-body system are determined by the mass and statistics of the constituents and by the potential energy surface. In many cases, the many-body potential energy surface can be approximated quite accurately by a sum of two-body potentials. The interaction strength g of the N -body system is then determined by the underlying two-body potential and, assuming N identical mass m particles, the mass m . The critical coupling constant $g_*^{(N)}$, for which the N -body cluster becomes unbound, defines the threshold. This paper investigates the near-threshold regime of bosonic three-dimensional N -body clusters, i.e., the regime where $g \gtrsim g_*^{(N)}$. This near-threshold regime is particularly interesting since some properties of the bosonic many-body system become independent of the details of the underlying potential energy surface, i.e., some properties of weakly-bound clusters consisting of N bosons become universal as $g \rightarrow g_*^{(N)}$ [1, 2, 3, 4, 5, 6, 7, 8, 9].

Our study includes the characterization of “super-borromean” N -body clusters [10]. Borromean trimers, which consist of three bosons for which each dimeric subsystem is unbound, have been studied in detail in the literature [11, 12, 13]. Super-borromean clusters, which consist of N bosons for which all subsystems with $N - n$, where $n = 1, \dots, N - 2$, are unbound, in contrast, have not been studied in much detail. To characterize these delicate systems, we perform precise diffusion Monte Carlo (DMC) calculations for clusters interacting additively through realistic shape-dependent two-body Van der Waals potentials. We determine the

critical coupling strengths $g_*^{(N)}$ for atomic clusters with up to $N = 40$ bosons and compare with variational bounds. The near-threshold behavior of weakly-bound three-dimensional bosonic clusters has been investigated in a series of papers before [2, 4, 7, 8]. We believe, however, that advances in the theoretical understanding, including predictions derived using effective theories and zero-range models [8, 14], and in the numerical treatment make it worthwhile to revisit the characterization of weakly-bound three-dimensional clusters. In particular, we present more accurate energies for a larger range of coupling strengths and for a larger range of cluster sizes than previous studies.

The present study is additionally motivated by recent experiments on extremely weakly-bound molecules created from ultracold Bose and Fermi gases. Utilizing Feshbach resonances the effective interaction strength between two atoms at ultracold temperatures can be changed essentially at will through application of an external magnetic field [15, 16]. The existence of this external knob has led to the observation of extremely weakly-bound diatomic molecules in highly-excited vibrational states [17, 18, 19] and provided evidence for the formation of Efimov trimer states [20, 21] in an ultracold environment. Furthermore, recent experiments on cold Cs atoms evidence the creation of larger weakly-bound clusters [22]; these experiments point towards Feshbach engineering of weakly-bound clusters. Feshbach resonances arise from the coupling of two Born-Oppenheimer potential curves through a hyperfine Hamiltonian and require, in general, a multi-channel description. In the case of a broad resonance, however, the change of the effective scattering length can be described within a single channel model [23]. Using a single channel approximation, this paper describes weakly-bound three-dimensional bosonic clusters with varying atom-atom scattering lengths with

up to $N = 40$ atoms.

Section II A describes the many-body Hamiltonian and the characteristics of the underlying two-body potential. Section II B is devoted to a discussion of our numerical approach to solving the many-body Schrödinger equation. Our results for the energetics and structural properties are presented in Secs. III and IV, respectively, and our conclusions in Sec. V.

II. SYSTEM AND NUMERICAL APPROACH

A. Many-body Hamiltonian

Consider the Hamiltonian H for N bosons with mass m ,

$$H = -\frac{\hbar^2}{2m} \sum_{j=1}^N \nabla_j^2 + \sum_{j < k}^N V(r_{jk}), \quad (1)$$

where ∇_j^2 and r_{jk} denote respectively the 3D Laplace operator of the j th boson and the internuclear distance between particles j and k . This Hamiltonian assumes a many-body potential energy surface written as a sum of atom-atom potentials $V(r)$. Our calculations are performed for a realistic Van der Waals triplet tritium-tritium potential [24, 25, 26, 27, 28, 29], which is repulsive at short interparticle distances r and falls off at large r as $\sum_{n=6,8,\dots} -C_n r^{-n}$. Figure 1 shows the tritium-tritium potential as a function of the interparticle distance r . The potential has a minimum of depth -4.6cm^{-1} at $r \approx 7.8a_0$, where a_0 denotes the Bohr radius. Solving the one-dimensional scaled radial Schrödinger equation shows that the tritium dimer has no bound state [10] (see also Sec. III A). The scattering length a ,

$$a = \lim_{k \rightarrow 0} -\frac{\tan(\delta(k))}{k}, \quad (2)$$

of the tritium dimer is negative, i.e., $a = -82.1a_0$ [10], which indicates that the dimer is only slightly short of binding. In Eq. (2), $\delta(k)$ denotes the energy-dependent s -wave phase shift and k the relative wave vector of the equivalent one-body problem with reduced mass $m/2$.

Our interest in this paper is in a detailed description of weakly-bound clusters with varying coupling constant near threshold. To change the coupling strength g of the cluster, we vary the atom mass m , i.e., we consider “artificial” clusters with atom masses that are heavier and lighter than the tritium mass. By rewriting the many-body Schrödinger equation in scaled units, it can be readily seen that changing the atom mass changes the coupling strength. For example, for systems interacting additively through Lenard-Jones potentials with well depth ϵ and length scale σ the coupling constant g is directly proportional to the atom mass, $g = 4m\epsilon\sigma^2/\hbar^2$.

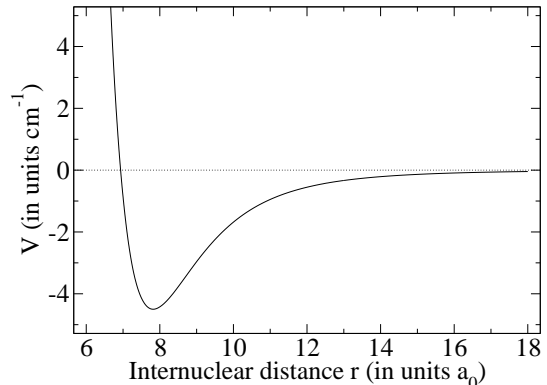


FIG. 1: Triplet tritium-tritium interaction potential as a function of the internuclear distance r .

As alluded to in the introduction, the coupling strength can be varied experimentally via a Feshbach resonance [30, 31]. Although a full description of a Feshbach resonance requires the coupling between at least two channels—in tritium, e.g., of the singlet and triplet potential curves (coupled through a long-range hyperfine Hamiltonian) [10, 32]—, some properties can be described within a single channel model. We thus envision that changing the atom mass in our single channel treatment can be mapped to changing the strength of an external magnetic field, and hence of the atom-atom scattering length, in the vicinity of a two-body Feshbach resonance. We expect that our calculations uncover the “generic” behaviors of three-dimensional bosonic Van der Waals clusters, which are interacting additively through two-body potentials with repulsive short-range core and long-range tail with leading $-C_6/r^6$ term. In particular, we believe that usage of a different two-body potential in Eq. (1) will result in the same qualitative but possibly different quantitative behaviors of weakly-bound bosonic clusters.

Pluses in Fig. 2 show the atom-atom scattering length a for the tritium-tritium potential as a function of the atom mass m . The scattering length a diverges at $m \approx 5933.4(2)m_e$, where m_e denotes the electron mass and the value in round brackets the uncertainty of m arising from the numerical determination of the scattering length a . Since this is the mass at which the dimer becomes unbound, we refer to this mass as the critical mass $m_*^{(2)}$ of the dimer. A vertical solid line in Fig. 2 marks the value of $m_*^{(2)}$. We find that the scattering length a vanishes for $m \approx 2311.0(2)m_e$. This mass value is indicated by a vertical solid line in Fig. 2 and puts an upper bound on the critical mass for the bulk system ($N \rightarrow \infty$), i.e., $m_*^{(\infty)} \leq 2311.0m_e$ [1]. This bound is obtained variationally by expanding the energy in terms of the density. For negative a , the leading order in the expansion becomes negative and the bulk system is nec-

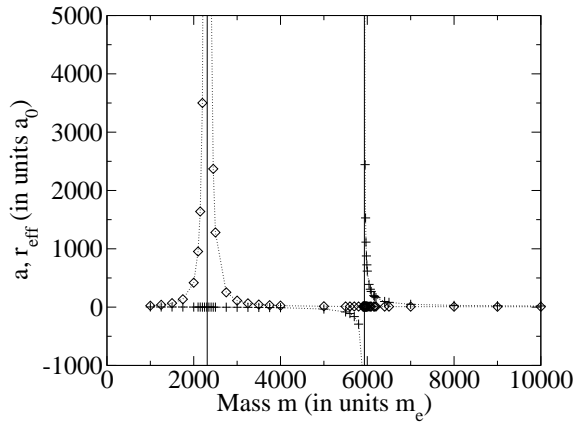


FIG. 2: Pluses and diamonds show the atom-atom scattering length a and the effective range r_{eff} , respectively, as a function of the atom mass m for the triplet tritium-tritium potential (see text). To guide the eye dotted lines connect the symbols. Vertical solid lines indicate the mass $m \approx 2311.0m_e$, at which a goes through zero, and the critical mass $m_*^{(2)} \approx 5933.4m_e$, at which the scattering length a diverges.

essarily bound [1]. Section III C compares our critical masses $m_*^{(N)}$ calculated for up to $N = 40$ atoms with the variational upper bound for $m_*^{(\infty)}$.

Diamonds in Fig. 2 show the effective range r_{eff} , which we calculate through the relationship

$$-\frac{1}{a(k)} \approx -\frac{1}{a} + \frac{1}{2}r_{eff}k^2, \quad (3)$$

as a function of the atom mass m . In Eq. (3), $a(k)$ denotes the energy-dependent scattering length, $a(k) = -\tan(\delta(k))/k$. The effective range is largest in the region where the two-body scattering length vanishes. In the region where a diverges, r_{eff} takes on values of the order of $10a_0$. The scattering length a , the effective range r_{eff} and the Van der Waals length r_{vdW} , where $r_{vdW} = (mC_6/\hbar^2)^{1/4}$, are the relevant length scales of the two-body problem near threshold. For a zero-range model with a single parameter, namely the scattering length a , to be applicable for $N = 2$, a needs to be the largest length scale in the problem. This condition can be expressed as

$$|E_2| \ll \min\left(\frac{\hbar^2}{mr_{eff}^2}, \frac{\hbar^2}{mr_{vdW}^2}\right), \quad (4)$$

where E_2 denotes the ground state energy of the dimer. For zero-range models to be applicable to clusters with $N > 2$, a condition similar to Eq. (4), possibly with an additional scaling factor N or $N(N-1)/2$, needs to be fulfilled.

B. Numerical treatment of N -body clusters

To determine the ground state energy and wave function of the two-body system [Eq. (1) with $N = 2$], we separate off the center of mass motion and scale the wave function for the interparticle distance to remove first derivative terms in the kinetic energy operator. The scaled one-dimensional radial Schrödinger equation can then be solved by diagonalizing the Hamiltonian using B-splines. To treat very weakly-bound dimers with varying mass m , we optimize the adaptive grid (i.e., the grid spacings, the number of grid points and the integration interval) for each mass. The upper integration limit is determined by the size of the bound state; integrating the Schrödinger equation out to roughly $100a$ leads to converged results for all two-body systems considered in Sec. III A.

The calculations of the trimer energies are, due to the larger number of degrees of freedom, more involved than those of the dimer energies. Separating off the center of mass motion reduces the nine-dimensional problem to a six-dimensional problem. Since we are in this paper primarily interested in ground state properties, we restrict ourselves to states with vanishing total angular momentum, i.e., $J = 0$. The resulting three-dimensional Hamiltonian can be written in terms of Whitten and Smith' hyperspherical coordinates [33], which allow the Bose symmetry to be accounted for readily. To solve the corresponding scaled Schrödinger equation, we expand the wave function in angle-dependent channel functions Φ , which depend parametrically on the hyperradius R , and a set of weight functions $F(R)$. Our numerical implementation is described in Ref. [34]. We check the convergence by changing the hyperangular grid, the hyperradial grid, the number of channel functions included in the expansion, and the step size used in the numerical determination of the derivatives of the channel functions. The trimer ground state energies presented in Sec. III B have an accuracy of a few percent. For selected trimers, we also report the first excited state energy with $J = 0$.

For cluster systems with more than a few atoms, basis set expansion-type techniques become computationally unfeasible. Consequently, we solve the many-body Schrödinger equation for $N \geq 4$ using alternative techniques, i.e., the variational quantum Monte Carlo (VMC) method and the DMC method with importance sampling [35]. Our numerical implementations follow Ref. [36]. The VMC method minimizes the energy of the cluster system by optimizing the many-body wave function, which is written in terms of a set of parameters \vec{p} . The optimized variational wave function ψ_T then enters our DMC calculations, which result in essentially exact ground state energies, as a guiding function. Due to the stochastic nature of the MC algorithms, the DMC energies reported in Sec. III C have statistical uncertainties.

We use two different functional forms for the variational wave function. For small clusters with about up

to $N = 10$ atoms, each atom has roughly the same average distance to all other atoms in the cluster. In this case, our variational wave function ψ_T is written as a product of pair wave functions ϕ [37],

$$\psi_T(\vec{r}_1, \dots, \vec{r}_N) = \prod_{j < k}^N \phi(r_{jk}), \quad (5)$$

where

$$\phi(r) = \exp \left[-\frac{p_{-5}}{r^5} - \frac{p_2}{r^{-2}} - p_0 \log(r) - p_1 r \right]. \quad (6)$$

For larger clusters, the variational wave function given in Eqs. (5) and (6) does not give a good variational energy and we additionally include a variational Fermi function which depends on the distance R_j of the j th atom to the center of mass of the cluster [38],

$$\psi_T(\vec{r}_1, \dots, \vec{r}_N) = \left[\prod_{j < k}^N \phi(r_{jk}) \right] \left[\prod_{l=1}^N \bar{\phi}(R_l) \right]. \quad (7)$$

Here, ϕ is given by Eq. (6) with $p_0 = p_1 = 0$ and

$$\bar{\phi}(R) = \left[1 + \exp \left(\frac{R - p_e}{p_\sigma} \right) \right]^{-1}. \quad (8)$$

The variational parameters p_e and p_σ determine the size of the cluster and the sharpness of the cluster's surface region, respectively. For each cluster system considered, we optimize the variational parameters by minimizing the energy expectation value $\langle \psi_T | H | \psi_T \rangle / \langle \psi_T | \psi_T \rangle$. The $3N$ -dimensional integrals are evaluated using the Metropolis algorithm. Our VMC energies, except for those for the systems closest to threshold (see Sec. III C), recover more than about 75-80% of the essentially exact DMC ground state energies.

The DMC calculations become computationally more demanding as we approach the threshold, since the kinetic and potential energy nearly cancel. In the near-threshold regime great care has to be taken to avoid any guiding function bias and to ensure convergence of the DMC calculations. To check that our DMC code describes extremely weakly-bound clusters accurately, we compare the DMC energies for the trimer with those calculated by the hyperspherical B-spline treatment. We find agreement to within the statistical uncertainty for $m \geq 6000m_e$ but do not obtain reliable DMC energies for significantly smaller masses.

Unlike the DMC energy expectation value, which is essentially exact (except for statistical uncertainties and possible time step errors), the expectation value of any structural quantity B is in the "standard" DMC algorithm calculated with respect to the mixed density,

$$\langle B \rangle_{DMC} = \langle \Psi | B | \psi_T \rangle / \langle \Psi | \psi_T \rangle. \quad (9)$$

Here, Ψ denotes the exact stationary ground state wave function [35]. To improve upon this mixed estimator,

we calculate the so-called extrapolated expectation value $\langle B \rangle_{ex}$ [39],

$$\langle B \rangle_{ex} = 2\langle B \rangle_{DMC} - \langle B \rangle_{VMC}, \quad (10)$$

where $\langle B \rangle_{VMC}$ denotes the VMC expectation value,

$$\langle B \rangle_{VMC} = \langle \psi_T | B | \psi_T \rangle / \langle \psi_T | \psi_T \rangle. \quad (11)$$

For the systems studied in this paper, the extrapolated expectation values $\langle B \rangle_{ex}$ are expected to be fairly close to the exact expectation values. Section IV reports expectation values for the pair distribution function $P(r)$ and the interparticle distance r .

III. ENERGETICS

This section presents our numerically determined energies for clusters with up to 40 atoms and their interpretation.

A. $N = 2$

Pluses in Fig. 3(a) show the absolute value of the s -wave ground state energies E_2 for two particles interacting through the triplet tritium-tritium potential for a number of different m , i.e., $m \in [5933.4m_e, 10000m_e]$. The tritium dimer itself is, as mentioned in Sec. II A, unbound. The ground state energies shown in Fig. 3 extend over nearly ten orders of magnitude; E_2 for the most weakly-bound dimer considered with $m = 5933.4$ is $-6 \times 10^{-11} \text{cm}^{-1}$, and that for the most strongly-bound dimer considered with $m = 10000m_e$ is -0.19cm^{-1} .

We can compare the numerically determined ground state energies E_2 with the energies E_2^δ predicted from a zero-range model, which supports a bound state for positive a ,

$$E_2^\delta = -\frac{\hbar^2}{ma^2}. \quad (12)$$

A solid line in Fig. 3(a) shows the absolute value of the zero-range energies E_2^δ . In the region where the zero-range model provides a good description of the dimer energies, the scattering length is the largest length scale in the problem, i.e., $a \gg r_{eff}$ and $a \gg r_{vdW}$ (see Fig. 2). As a becomes comparable to r_{eff} , the energies E_2^δ deviate visibly from the exact energies E_2 and Eq. (12) has to be modified to account for the dependence of the energy on the effective range r_{eff} in addition to a .

We now describe an analysis that allows an accurate determination of the critical mass $m_*^{(2)}$ from the two-body ground state energies. In principle, this analysis is not needed since our scattering length calculations allow the critical mass $m_*^{(2)}$ to be determined with high accuracy (see Sec. II A). The analysis presented in the next two paragraphs for $N = 2$ is meant as a test of principle;

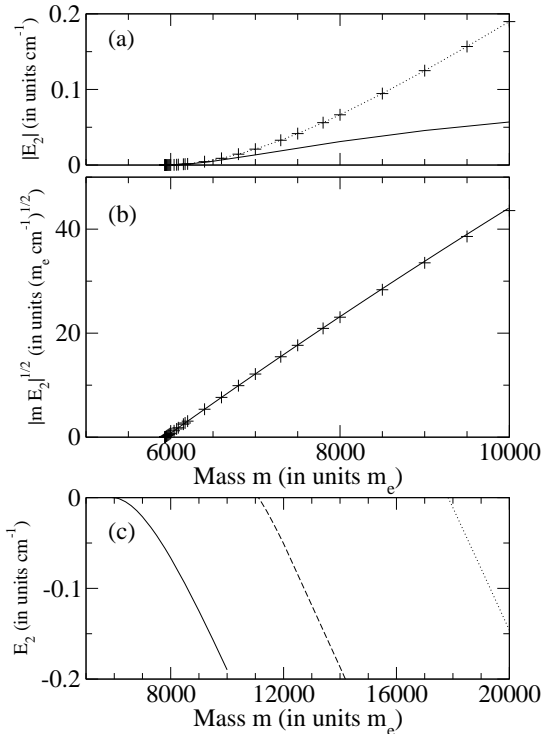


FIG. 3: (a) Pluses show the absolute value of the numerically determined two-body ground state energies E_2 as a function of the atom mass m . To guide the eye, a dotted line connects the symbols. For comparison, a solid line shows the absolute value of the two-body energies E_2^0 , Eq. (12), obtained from the scattering length a . (b) Pluses show the scaled dimer ground state energies $\sqrt{m|E_2|}$ as a function of the atom mass m . The scaled energies $\sqrt{m|E_2|}$ vary to first order linearly with m . A solid line shows our fit to the scaled energies $\sqrt{m|E_2|}$, treating $c_1^{(2)}$, $c_2^{(2)}$ and $m_*^{(2)}$ as fitting parameters (see text). (c) Solid, dashed and dotted lines show the lowest two-body energies for $l = 0, 1$ and 2 , respectively, as a function of the atom mass m . Note that the mass range shown in the lowest panel differs from the mass ranges shown in the upper two panels.

an analogous analysis is in Secs. III B and III C applied to larger clusters. For $N = 3$, accurate calculations of the dimer plus atom scattering length can be performed but are not pursued here. For $N > 3$, however, only approximate calculations for the $N - 1$ plus atom scattering length have been performed to date [5, 40].

Within effective range theory, the two-body ground state energies E_2 near threshold are determined by Taylor-expanding the logarithmic derivative of the bound state wave function about the critical mass $m_*^{(2)}$ [41, 42],

$$\sqrt{m|E_2|} = \sum_{i=1}^{\infty} c_i^{(2)} (m - m_*^{(2)})^i, \quad (13)$$

where the $c_i^{(2)}$ denote expansion coefficients. Pluses

N	$m_*^{(N)}$ [m_e]	$c_1^{(N)}$ [$\sqrt{\text{cm}^{-1}/m_e}$]	$c_2^{(N)}$ [$\sqrt{\text{cm}^{-1}/m_e^3}$]
2	5933.5(1)	0.011623(2)	$-2.243(5) \times 10^{-7}$
3	5352(17)	0.026(2)	$-2.6(6) \times 10^{-6}$
4	4836(08)	0.033(1)	$-1.9(2) \times 10^{-6}$
5	4527(15)	0.042(2)	$-3.2(6) \times 10^{-6}$
6	4311(18)	0.051(2)	$-4.2(9) \times 10^{-6}$
7	4097(06)	0.056(1)	$-3.7(4) \times 10^{-6}$
8	3992(09)	0.067(2)	$-7.0(9) \times 10^{-6}$
9	3867(16)	0.072(3)	$-6.6(1.7) \times 10^{-6}$
10	3789(14)	0.084(4)	$-1.0(3) \times 10^{-5}$
20	3142(26)	0.090(8)	$-1.4(6) \times 10^{-5}$
40	2919(13)	0.202(7)	$-2.9(6) \times 10^{-5}$

TABLE I: Fitting parameters $m_*^{(N)}$, $c_1^{(N)}$ and $c_2^{(N)}$ for three-dimensional bosonic clusters with $N = 2 - 10, 20$ and 40 interacting additively through a triplet tritium-tritium potential. The numbers in brackets indicate the uncertainties of the fit, neglecting possible uncertainties of the energies (see text).

in Fig. 3(b) show the scaled energies $\sqrt{m|E_2|}$, which vary roughly linearly with m . Close inspection, however, reveals deviations from a linear behavior. This indicates that the first term in the expansion given by Eq. (13) is dominant, but that the second expansion coefficient $c_2^{(2)}$ contributes non-negligibly. To determine $m_*^{(2)}$, $c_1^{(2)}$ and $c_2^{(2)}$, we fit our scaled energies for $m \in [5933.4m_e, 10000m_e]$ to the first two terms of the expansion given by Eq. (13). The resulting fit with $m_*^{(2)} = 5933.5(1)m_e$, $c_1^{(2)} = 1.1623(2) \times 10^{-2} \sqrt{\text{cm}^{-1}/m_e}$ and $c_2^{(2)} = -2.243(5) \times 10^{-7} \sqrt{\text{cm}^{-1}/m_e^3}$ (see Table I) agrees well with the exact energies and is shown by a solid line in Fig. 3(b). The numbers in round brackets indicate the uncertainty of the fitting parameters, excluding possible numerical inaccuracies of the two-body energies. The critical mass extracted by fitting to the dimer bound state energies is in excellent agreement with the critical mass $m_*^{(2)} = 5933.4(2)m_e$ determined from the scattering length calculations (see Sec. II A).

The calculations for larger clusters necessarily cover, due to numerical difficulties, a smaller range of energies, i.e., we are not able to perform bound state calculations as close to threshold as for the dimer. Furthermore, our cluster energies for $N > 3$ can only be determined within a statistical uncertainty, which adds an additional complication. If we exclude the two-body energies very close to threshold from our fit, i.e., if we perform a fit to the scaled energies with $m \in [6800m_e, 10000m_e]$ (which is roughly comparable to the corresponding ranges considered for $N \geq 3$, see Secs. III B and III C), we find a critical mass $m_*^{(2)} = 5932.1(8)m_e$, where the uncertainty in brackets reflects, as above, the uncertainty of the fit. Since $c_2^{(2)}$ is negative the critical mass predicted by this fit, which excludes the energies closest to threshold, is expected to be smaller than the exact threshold value. The deviation from the fit that includes the whole mass

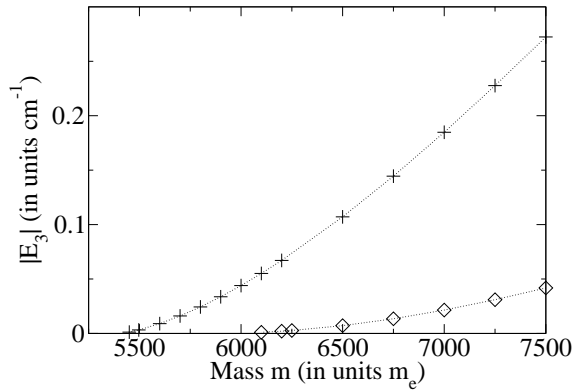


FIG. 4: Pluses and diamonds show respectively the absolute value of the ground state and first excited state energies with $J = 0$ of the trimer as a function of the atom mass m . To guide the eye, dotted lines connect the symbols.

range (see above) is about $1.5m_e$, thus providing us with an estimate of the error made when extracting the critical mass from a set of energies, which excludes the very near-threshold regime.

None of the dimers considered in this subsection supports an excited $l = 0$ state, where l denotes the orbital angular momentum quantum number. Some of the dimers do, however, support rotationally excited states with $l > 0$. Even l states are allowed for bosons and fermions with opposite spin, and odd l states for spin-aligned fermions. Figure 3(c) shows the two-body bound state energies for $l = 0$ (solid line), $l = 1$ (dashed line) and $l = 2$ (dotted line) as a function of the atom mass m . The near-threshold behavior of the $l > 0$ states is, due to the presence of the angular momentum barrier of the effective potential, distinctly different from that of the $l = 0$ states (for which the angular momentum barrier vanishes). The next subsection discusses the energetics of the trimer.

B. $N = 3$

Pluses in Fig. 4 show the absolute value of the trimer ground state energies, obtained by solving the Schrödinger equation using hyperspherical coordinates (see Sec. II B), as a function of the atom mass m . The ground state energies E_3 extend over nearly three orders of magnitude. The most weakly-bound trimer considered with $m = 5430m_e$ has a ground state energy of $-4.8 \times 10^{-4}\text{cm}^{-1}$, and the most strongly-bound trimer considered with $m = 7500m_e$ has a ground state energy of -0.27cm^{-1} .

As in the dimer case, we fit the scaled energies $\sqrt{m|E_3|}$ to the expansion given in Eq. (13) with $c_i^{(2)}$ ($i \leq 2$) and $m_*^{(2)}$ replaced by $c_i^{(3)}$ and $m_*^{(3)}$, respectively. The result-

ing fitting parameters $c_1^{(3)}$, $c_2^{(3)}$ and $m_*^{(3)}$ are given in Table I. The fit, shown by a solid line in Fig. 5(b), describes the trimer energies quite well. Since the trimer contains three “dimer bonds”, the critical mass $m_*^{(3)}$ for the trimer is significantly smaller than that for the dimer. The parameter $c_2^{(N)}$, which quantifies the non-linear dependence of the scaled energies on the mass m , is about an order of magnitude more negative for the trimer than for the dimer. The negative value of $c_2^{(3)}$ suggests that the critical mass $m_*^{(3)}$ predicted by our fit is somewhat smaller than the true threshold value, which could be determined more precisely if we were able to calculate accurate energies closer to threshold. The smallest mass for which we reliably determine a negative trimer energy provides an upper bound for the critical mass $m_*^{(3)}$. We believe that the lower bound, i.e., the critical mass predicted by our fit, is more accurate than this upper bound.

Diamonds in Fig. 4 show the first excited state energy $E_3^{(1)}$ with $J = 0$ as a function of m . Although the mass at which the excited state becomes unbound is larger than that at which the ground state becomes unbound, the excited state energies approach the threshold in qualitatively the same way as the ground state energies do. In fact, the excited state of the helium trimer, which is an Efimov state [3], was for a long time considered to be the possibly most promising candidate for observing universal behaviors experimentally [43]. Just as the near-threshold behavior of the excited dimer states with $l > 0$ is qualitatively different from that of the $l = 0$ state [see Fig. 3(c)], the near-threshold behavior of trimer states with $J \neq 0$ is predicted to be qualitatively different from that of the $J = 0$ states [44].

C. $N \leq 40$

We now turn to the discussion of weakly-bound clusters with up to $N = 40$ atoms. Symbols in Fig. 5(a) show the absolute value of the ground state energies E_N/N per particle as a function of the atom mass m for $N = 2 - 10$. The energies for $N = 2$ and 3 are also shown in Figs. 3 and 4, respectively. The statistical uncertainties of the DMC energies E_N/N per particle, $N \geq 4$, are not shown in Fig. 5 since they are smaller than the symbol sizes. The overall behavior of the ground state energies is similar for all N . Below, we use our energies for $N = 2 - 10$ (see Fig. 5), and $N = 20$ and 40 (not shown) to determine the critical masses $m_*^{(N)}$.

Symbols in Fig. 5(b) show the scaled energies $\sqrt{m|E_N|/N}$ for $N = 2 - 10$ as a function of the atom mass m . To determine the critical masses $m_*^{(N)}$, we fit the scaled energies $\sqrt{m|E_N|}$ for each N to the functional form given in Eq. (13) with $c_i^{(2)}$ ($i \leq 2$) and $m_*^{(2)}$ replaced by $c_i^{(N)}$ and $m_*^{(N)}$, respectively. The resulting fitting parameters $c_1^{(N)}$, $c_2^{(N)}$ and $m_*^{(N)}$ are given in Ta-

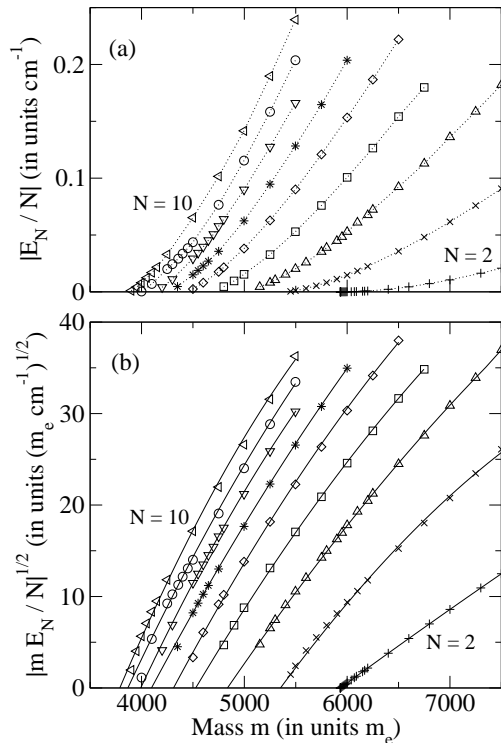


FIG. 5: (a) Symbols show the absolute value of the numerically determined ground state energies E_N/N per particle as a function of the atom mass m for $N = 2 - 10$; the energies for $N = 2$ and 3 are also shown in Figs. 3 and 4, respectively. To guide the eye, dotted lines connect energies for the same N . (b) Symbols show the scaled energies $\sqrt{m}|E_N/N|$ as a function of the atom mass for $N = 2 - 10$. Solid lines show our fits to the scaled energies treating $c_1^{(N)}$, $c_2^{(N)}$ and $m_*^{(N)}$ as fitting parameters. For each N , the crossing point of the fit with the zero-energy line predicts the critical mass $m_*^{(N)}$.

ble I; $c_1^{(N)}$ increases with increasing N , and $m_*^{(N)}$ decreases with increasing N . The fitting parameter $c_2^{(N)}$ is negative for all N considered; its largest uncertainty is about 40% for $N = 20$. As discussed in Sec. III B, the critical masses $m_*^{(N)}$ predicted by our fits are expected to be lower bounds to the exact threshold value. An upper bound is given by the smallest mass for which we report a bound state. A more precise extrapolation of the threshold value is complicated by the fact that the DMC energies have error bars and that the determination of the energy becomes numerically more demanding the closer the system's mass is to the critical mass $m_*^{(N)}$.

Asterisks in Fig. 6(a) show the critical masses $m_*^{(N)}$ predicted by our fits for $N = 2 - 10, 20$ and 40 as a function of $1/N$. A diamond in Fig. 6(a) shows the upper bound for the critical mass $m_*^{(\infty)}$ of the bulk system, i.e., $m_*^{(\infty)} = 2311.0m_e$ (see Sec. II A). We choose the $1/N$ -scale since it allows the critical mass for the dimer and the bulk system to be shown on the same graph; to

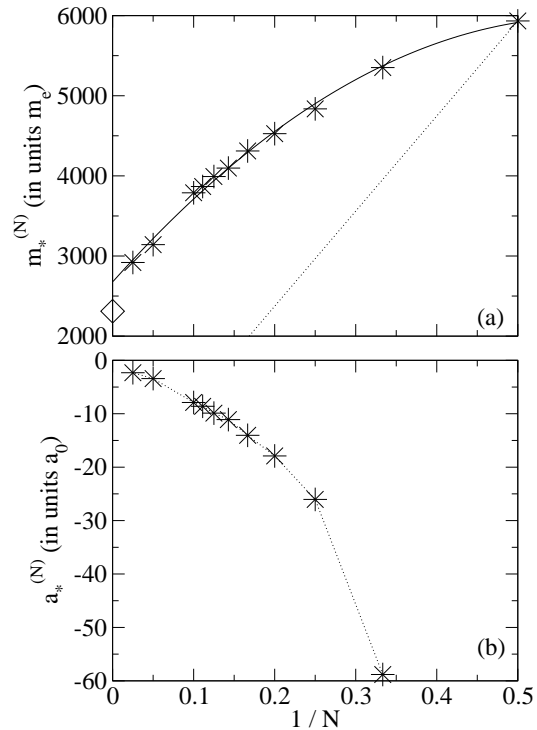


FIG. 6: (a) Asterisks show the critical masses $m_*^{(N)}$, predicted by our fits to the scaled ground state energies $\sqrt{m}|E_N/N|$, as a function of $1/N$ for $N = 2 - 10, 20$ and 40 . The diamond shows an upper bound for the critical mass $m_*^{(\infty)}$ of the bulk system and the solid line shows our three-parameter fit, Eq. (14), with $D = 2676(47)m_e$, $E = 11325(458)m_e$ and $F = -9696(852)m_e$ to the critical masses $m_*^{(N)}$ (the numbers in round brackets denote the uncertainty of the fit, neglecting possible uncertainties of the critical masses). The dotted line shows a lower bound for $m_*^{(N)}$ using the equal sign in the relationship $m_*^{(N)} \geq m_*^{(N-1)}(N-1)/N$ and $m_*^{(2)} = 5933.4m_e$. As expected, our numerically determined critical masses lie above this analytical bound. (b) Asterisks show the critical scattering length $a_*^{(N)}$ as a function of $1/N$ for $N = 2 - 10, 20$ and 40 . To guide the eye, a dotted line connects the symbols.

the best of our knowledge, the functional dependence of $m_*^{(N)}$ on the system size is unknown. Our critical mass for $N = 40$ is significantly larger than the upper bound $m_*^{(\infty)}$ determined variationally for the bulk system. Indeed, a three-parameter fit of the form

$$m_*^{(N)} = D + E/N + F/N^2 \quad (14)$$

to our critical masses for up to 40 atoms, shown by a solid line in Fig. 6(a), predicts a larger critical mass for the bulk system than the upper bound $m_*^{(\infty)} = 2311.0m_e$ at which the scattering length crosses zero. We speculate that our calculations for comparatively small N cannot be used to extrapolate $m_*^{(\infty)}$ reliably since the ratio of bulk to surface atoms increases appreciably with increas-

ing N . Furthermore, our extrapolated critical masses have non-negligible uncertainties. To connect the results discussed here to a realistic physical system, we note that homogeneous atomic spin-polarized hydrogen, which has an atom mass of $m = 1837m_e$ and interacts through a sum of two-body potentials only slightly different from that considered here, exists under normal pressure as a gas and not as a liquid [45].

The critical mass $m_*^{(N)}$ of the N -body system is bounded by the critical mass of the system with $N - 1$ particles through $m_*^{(N)} \geq m_*^{(N-1)}(N - 1)/N$ [13]. A dotted line in Fig. 6(a) shows this lower bound, assuming $m_*^{(2)} = 5933.4m_e$. Figure 6(b) indicates that this analytical estimate provides a weak bound for all bosonic systems considered here. An upper bound is given by $m_*^{(N)} = m_*^{(N-1)}$.

To relate our critical masses to an experimentally tunable parameter, we calculate the scattering length for each $m_*^{(N)}$ and refer to it as the critical scattering length $a_*^{(N)}$. Asterisks in Fig. 6(b) show the critical scattering length $a_*^{(N)}$ as a function of $1/N$. Figure 6(b) suggests that Borromean trimers exist for $a \leq -58.8a_0$ and Borromean tetramers for $a \in [-58.8a_0, -26.0a_0]$. Investigation of the stability of these weakly-bound Borromean states is beyond the scope of this paper.

D. Correlations

We now investigate correlations between energies of the three- and four-particle systems. The description of universal properties of the trimer [9], such as the description of Efimov states, requires two parameters, a two-body momentum scale $\mu^{(2)}$ (typically taken to be inversely proportional to the s -wave scattering length a) and a three-body momentum scale $\mu^{(3)}$ (in some studies, the three-body parameter Λ_* is used instead [46, 47]). While the universal behaviors of the trimer are quite well understood [9], much less is known about those of larger systems. For example, although one expects a new momentum scale $\mu^{(4)}$ to be needed for the description of universal properties of the tetramer [14, 48], there is evidence that at least some observables of the tetramer near threshold are independent of this new momentum scale [8]. In this context, a number of studies have focused on the Tjon line [4, 49, 50, 51, 52], which was first investigated in nuclear physics and refers to the approximately linear correlation between the energies of the four-nucleon and the three-nucleon system [51, 52]. In the following, correlations between our trimer and tetramer energies, which are calculated for realistic atom-atom interactions, are demonstrated.

Pluses in Figs. 7(a) and (b) show the ratio between the ground state energies E_4 and E_2 as a function of the ratio between the ground state energies E_3 and E_2 on a linear and double-logarithmic scale, respectively. Unlike in Tjon's original work for fixed dimer energy [51, 52],

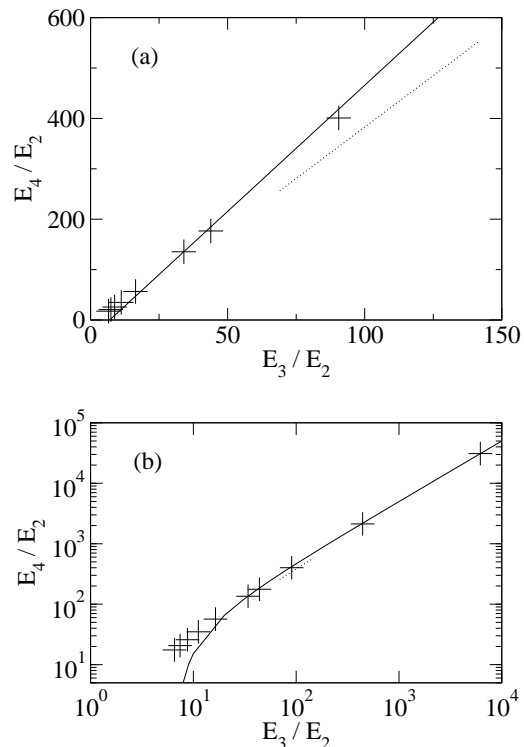


FIG. 7: Pluses show the energy ratio E_4/E_2 as a function of the energy ratio E_3/E_2 (E_4 , E_3 and E_2 denote ground state energies) on (a) a linear scale and (b) a log-log scale. Solid lines show our two-parameter fit (see text). Dotted lines show the result obtained within an effective quantum mechanical approach [8]. The data with the largest energy ratios correspond to systems closest to threshold, and those with the smallest energy ratios correspond to systems farthest away from threshold.

we scale the trimer and tetramer energies in Fig. 7 by the dimer energy since E_2 depends on the atom mass m . For each data point, the ground state energies E_2 , E_3 and E_4 are calculated for the same atom mass m . The systems closest to threshold are those with the largest energy ratios. For the smallest mass, $m = 5950m_e$, included in Fig. 7(b), the absolute value of E_2 is nearly four orders of magnitude smaller than that of E_3 , and more than four orders of magnitude smaller than that of E_4 . A two-parameter fit of the form $E_4/E_2 = B_3 + C_3 E_3/E_2$, shown by solid lines in Figs. 7(a) and (b), describes the dependence of E_4/E_2 on E_3/E_2 quite well (especially for systems close to threshold), thus confirming the existence of the Tjon line for atomic clusters. In particular, we find $B_3 = -34.9(8.3)$ and $C_3 = 5.008(5)$ (see also Table II), where the numbers in brackets indicate the uncertainty of the fit, neglecting possible inaccuracies of the energy ratios.

For comparison, dotted lines in Figs. 7(a) and (b) show a result derived within an effective quantum mechanics approach applied to bosonic clusters with $N = 2 - 4$

helium atoms [8]. This study finds $B_3 = -24.752$ and $C_3 = 4.075$ for $69 \leq E_3/E_2 \leq 142$. This range of E_3/E_2 values is significantly smaller than that considered in the present paper [solid lines in Figs. 7(a) and (b)]. The slope of the Tjon line derived within the effective quantum mechanical approach, applied to helium clusters, is somewhat smaller than our slope, which is derived from a series of numerical calculations for weakly-bound Van der Waals clusters. We find that our slope decreases if we perform a fit that excludes energy ratios for systems very close to threshold. This may explain the discrepancy between the results obtained within the two approaches.

It has been argued that, if the four-body momentum scale $\mu^{(4)}$ coincides with the three-body momentum scale $\mu^{(3)}$ [14], the slope of the Tjon line is about five. This argument suggests that the systems studied in the present paper have approximately equal three- and four-body momentum scales. It has further been suggested that the existence of equal three- and four-body momentum scales can be traced back to the repulsive core of the two-body interactions [14]. This interpretation suggests that the Tjon line is roughly five for all atomic systems near threshold and that the ground state energy of any weakly-bound tetramer interacting additively through Van der Waals potentials with repulsive core can be estimated quite reliably if the corresponding dimer and trimer ground state energies are known. This interpretation could be checked more rigorously by performing a series of calculations for systems interacting additively through a shape-dependent two-body potential, which depends on a parameter that controls the softness of the repulsive short-range part of the potential. For a “soft” repulsive core, the four-body momentum scale should deviate from the three-body scale and the slope of the Tjon line should deviate from five. Such a study is beyond the scope of this paper.

We now consider correlations between the tetramer ground state energy E_4 and the trimer excited state energy $E_3^{(1)}$, both scaled by the dimer ground state energy E_2 . Pluses in Fig. 8 show the energy ratio E_4/E_2 as a function of the energy ratio $E_3^{(1)}/E_2$ on a linear scale. A solid line shows our two-parameter fit $E_4/E_2 = \tilde{B}_3 + \tilde{C}_3 E_3^{(1)}/E_2$ with $\tilde{B}_3 = -558(35)$ and $\tilde{C}_3 = 565(29)$, while a dotted line shows that derived in Ref. [8] for $1.54 \leq E_3^{(1)}/E_2 \leq 2$ with $\tilde{B}_3 = -742.0$ and $\tilde{C}_3 = 645.1$. The agreement of the slopes, derived within two different frameworks and applied to two different systems, is quite reasonable. We now use the linear dependence of E_4/E_2 on E_3/E_2 and of E_4/E_2 on $E_3^{(1)}/E_2$ to predict the slope \tilde{C}_3 for the linear dependence of E_3/E_2 on $E_3^{(1)}/E_2$, $E_3/E_2 = \tilde{B}_3 + \tilde{C}_3 E_3^{(1)}/E_2$. From our slopes C_3 and \tilde{C}_3 , we obtain $\tilde{C}_3 = 112(6)$. For comparison, a fit to our data gives $\tilde{C}_3 = 124(5)$. The good agreement lends support to the predictive power of the approximately linear correlations between energy ratios of clusters with varying number of atoms.

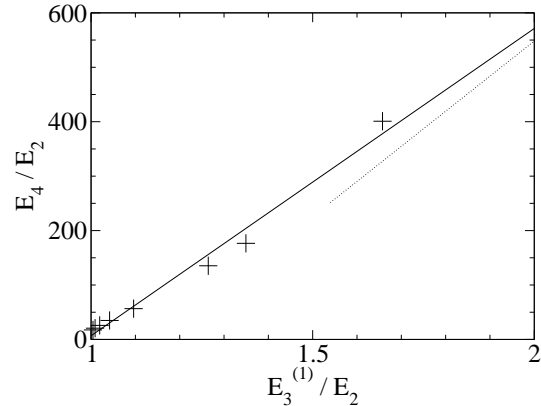


FIG. 8: Pluses show the energy ratio E_4/E_2 as a function of the energy ratio $E_3^{(1)}/E_2$ on a linear scale (E_2 and E_4 denote ground state energies, and $E_3^{(1)}$ denotes the first excited state energy with $J = 0$). A solid line shows our two-parameter fit (see text). A dotted line shows the results obtained within an effective quantum mechanical approach [8]. The data with the largest energy ratios correspond to systems closest to threshold, and those with the smallest energy ratios correspond to systems farthest away from threshold.

Correlations between the energies of two clusters differing in size by one atom, i.e., a linear relationship of the form $E_{N+1} = b_N + c_N E_N$, have been predicted analytically based on a separable approximation scheme for any cluster size [53] and numerically by performing variational calculations for small mixed ${}^3\text{He}_i\text{-}{}^4\text{He}_j$ clusters with $i + j \leq 5$ [50]. We find that our energies of clusters differing in size by one atom are not well described by such a linear two-parameter fit. If we instead scale, as in the investigation of the correlations between the tetramer and trimer energies, our ground state energies of the $(N + 1)$ - and N -atom clusters by the energy of the $(N - 1)$ -atom cluster, we find an approximately linear relationship. Pluses in Figs. 9(a)-(f) show the energy ratios E_{N+1}/E_{N-1} as a function of E_N/E_{N-1} for $N = 4 - 9$, and solid lines a linear fit of the form $E_{N+1}/E_{N-1} = B_N + C_N E_N/E_{N-1}$. The fitting parameters B_N and C_N are summarized in Table II. We refer to the approximately linear dependence of the energy ratios of clusters, which is illustrated in Fig. 9, as generalized Tjon lines. It will be interesting to investigate the implications of the behaviors of these generalized Tjon lines for the universal properties of weakly-bound bosonic clusters.

IV. STRUCTURAL PROPERTIES

This section presents selected structural properties of weakly-bound bosonic clusters in their ground state. The expectation values for $N \geq 4$ are calculated using the MC estimator given in Eq. (10). Figure 10 shows the pair

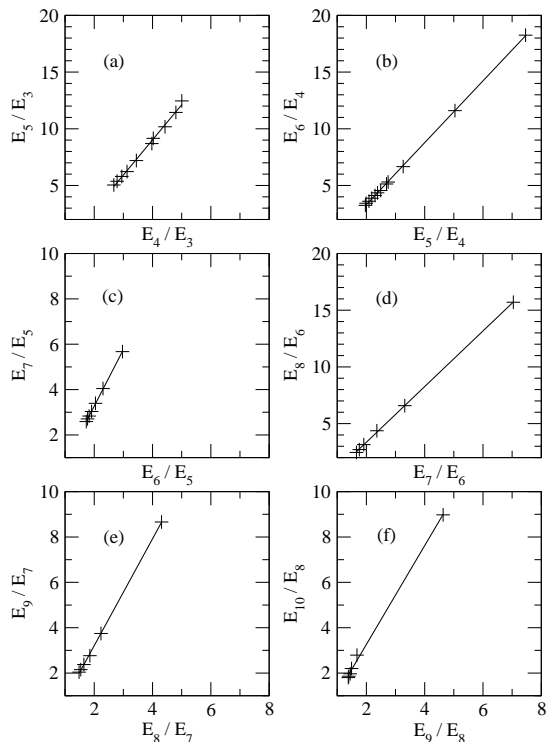


FIG. 9: Pluses show the energy ratio E_{N+1}/E_{N-1} as a function of the energy ratio E_N/E_{N-1} for (a) $N = 4$, (b) $N = 5$, (c) $N = 6$, (d) $N = 7$, (e) $N = 8$, and (f) $N = 9$. Solid lines show linear fits of the form $E_{N+1}/E_{N-1} = B_N + C_N E_N/E_{N-1}$ (see text). Note that the range of the vertical axis extends from 1 to 8 in all panels while that of the horizontal axis varies.

distribution function $P(r)$ for $N = 4$ and four different masses, i.e., $m = 5950m_e$, $5750m_e$, $5400m_e$ and $5150m_e$. The pair distribution function $P(r)$ indicates the likelihood of finding two particles at a distance r from each other and is normalized so that

$$\int_0^\infty P(r) r^2 dr = 1. \quad (15)$$

As the mass decreases, the maximum of $P(r)$, which is located at $r \approx 10a_0$, decreases. Furthermore, the pair distribution functions extend to significantly larger r values for small m than for large m . For example, the largest interparticle distance sampled in our DMC runs for $m = 5950m_e$ is $r \approx 100a_0$ while that for $m = 5150m_e$ is $r \approx 200a_0$. We find that the densities, not shown, of the weakly-bound clusters studied in this paper are structureless and do not possess any shell structure. The highly-diffuse clusters can thus be most appropriately thought of as “diffuse liquid blobs”.

To compare the structural behaviors of clusters with

N	B_N	C_N
3	-34.9(8.3)	5.008(5)
4	-3.37(27)	3.10(8)
5	-2.27(08)	2.78(2)
6	-1.71(03)	2.49(2)
7	-1.55(07)	2.45(2)
8	-1.50(06)	2.36(3)
9	-1.11(11)	2.18(5)

TABLE II: Fitting parameters B_N and C_N for $N = 3 - 9$. Numbers in brackets denote the uncertainty of the two-parameter fit $E_{N+1}/E_{N-1} = B_N + C_N E_N/E_{N-1}$, neglecting possible uncertainties of the energy ratios.

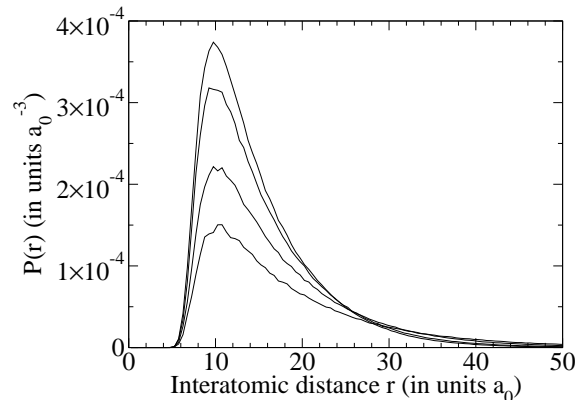


FIG. 10: Pair distribution functions $P(r)$ as a function of the interparticle distance r for $N = 4$ and four different masses, i.e., $m = 5950m_e$, $5750m_e$, $5400m_e$ and $5150m_e$ (from top to bottom). The pair distribution functions are calculated using the MC estimator given in Eq. (10), which combines the VMC and DMC expectation values. Statistical uncertainties are not shown for clarity.

different N , symbols in Fig. 11 show the expectation values of the interparticle distance r for clusters in the ground state with $N = 2 - 10$ (denoted by $\langle r \rangle_N$) as a function of the atom mass m . For fixed N , $\langle r \rangle_N$ decreases, as expected, with decreasing mass m . For a given mass, $\langle r \rangle_N$ decreases with increasing N . This behavior is consistent with the fact that the energy per particle for fixed mass decreases with increasing N . Furthermore, for fixed m , the expectation values $\langle r \rangle_N$ should reach a constant in the large N limit. Indeed, Fig. 11 indicates that the difference between $\langle r \rangle_N$ for two clusters differing in size by one atom is smaller for large than for small N .

It has been suggested that scaling functions, which allow the structural properties of the tetramer to be expressed in terms of expectation values of the dimer and trimer, exist [14]; the exact functional forms are, however, to the best of our knowledge unknown. Symbols in Fig. 12 show the ratio $\langle r \rangle_4 / \langle r \rangle_2$ as a function of the ratio $\langle r \rangle_3 / \langle r \rangle_2$. For each data point, the expectation val-

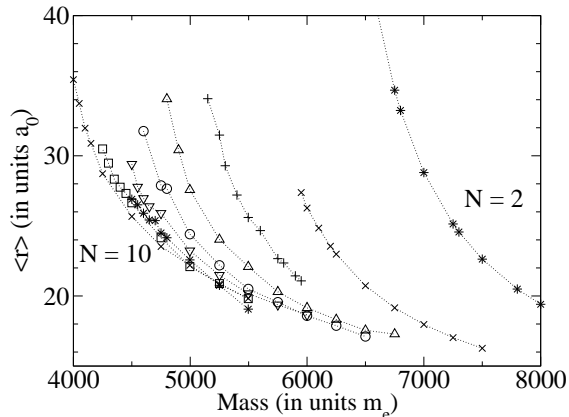


FIG. 11: Expectation value $\langle r \rangle_N$ of the interparticle distance for clusters in the ground state with $N = 2 - 10$ (from right to left) as a function of the atom mass m . The expectation values for $N \geq 4$ are calculated using the extrapolated estimator, Eq. (10), which combines the VMC and DMC expectation values. Errorbars, not shown, are at most about three times as large as the symbol sizes.

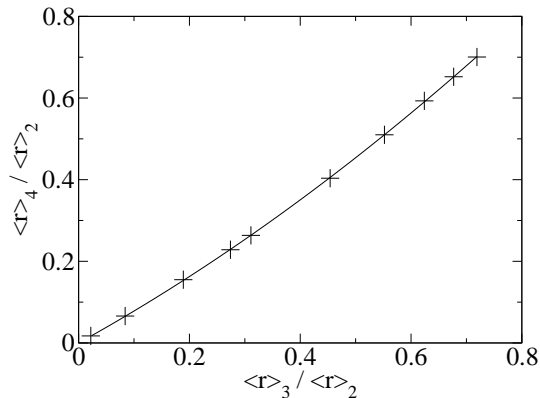


FIG. 12: Ratio $\langle r \rangle_4 / \langle r \rangle_2$ as a function of the ratio $\langle r \rangle_3 / \langle r \rangle_2$. Pluses show our numerically determined ratios while the solid line shows a two-parameter fit (see text).

ues $\langle r \rangle_4$, $\langle r \rangle_3$ and $\langle r \rangle_2$ are calculated for the same mass. The errorbars, not shown, are smaller than twice the size of the symbols. These ratios are well described by a two-parameter fit of the form $\langle r \rangle_4 / \langle r \rangle_2 = G \langle r \rangle_3 / \langle r \rangle_2 + H (\langle r \rangle_3 / \langle r \rangle_2)^2$ with $G = 0.751(5)$ and $H = 0.313(7)$ (solid line). We hope that the structural properties presented here will stimulate and aid further studies of weakly-bound bosonic clusters.

V. CONCLUSION

The physics of weakly-bound few-body systems can experimentally be investigated using ultracold atomic

gases. Indeed, the observation of resonances in an ultracold Bose gas has recently been interpreted as evidence for the presence of loosely-bound Efimov trimers [21]. Resonances associated with tetramers have also been reported [22]. These experiments may just be the beginning of detailed studies of the rich behaviors of few-body systems under controlled conditions. On the theoretical side, little is known about the universal near-threshold behaviors of three-dimensional systems with more than three particles. The reason is that analytical treatments become increasingly more complex as the number of degrees of freedom increases. On the other hand, numerical treatments are complicated by the fact that the kinetic and potential energy nearly cancel, thus requiring both to be calculated with high accuracy.

This paper presents a detailed study of the near-threshold behaviors of weakly-bound three-dimensional bosonic clusters with up to 40 atoms, for which the underlying potential energy surface is written as a sum of realistic Van der Waals atom-atom potentials with short-range repulsion and attractive long-range tail. In particular, we determine the critical mass $m_*^{(N)}$ for clusters with $N = 2 - 10, 20$ and 40 by performing calculations for each cluster as a function of the atom mass m . To the best of our knowledge, these are the first calculations that attempt an accurate determination of the critical coupling strengths of clusters with up to 40 atoms. Our critical masses are compared to analytical bounds. Furthermore, we show that our numerically determined three- and four-particle energies, scaled by the corresponding dimer energies, fall on the Tjon line. We present numerical evidence that the scaled energies of larger clusters differing in size by one atom also correlate linearly, i.e., the energy ratios fall on what we refer to as generalized Tjon lines. Motivated by a recent calculation based on zero-range models [14], we speculate that all atomic cluster systems show similar near-threshold behaviors. Finally, we present selected structural properties of weakly-bound few-body systems.

In closing, we emphasize that the near-threshold behavior of clusters crucially depends on the dimensionality. For example, the near-threshold behavior of weakly-bound two-dimensional few-body systems [54, 55] is very different from that presented here for three-dimensional systems. We hope that our work will stimulate further experimental and theoretical work on weakly-bound clusters.

We thank Chris Greene for fruitful discussions. Acknowledgement is made to the Donors of The Petroleum Research Fund, administered by the American Chemical Society, and the NSF (grant ITR-0218643) for support of this research.

-
- [1] L. W. Bruch, Phys. Rev. B **13**, 2873 (1976).
- [2] M. L. Cramer, L. W. Bruch, and F. Cabral, J. Chem. Phys. **67**, 1442 (1977).
- [3] T. K. Lim, S. K. Duffy, and W. C. Damer, Phys. Rev. Lett. **38**, 341 (1977).
- [4] T. K. Lim, S. Nakaichi, Y. Akaishi, and H. Tanaka, Phys. Rev. A **22**, 28 (1980).
- [5] S. Nakaichi-Maeda, and T. K. Lim, Phys. Rev. A **28**, 692 (1983).
- [6] S. K. Adhikari, A. Delfino, F. Frederico, I. D. Goldman, and L. Tomio, Phys. Rev. A **37**, 3666 (1988).
- [7] S. Moszkowski, S. Fleck, A. Kriek, L. Theußl, J.-M. Richard, and K. Varga, Phys. Rev. A **62**, 032504 (2000).
- [8] L. Platter, H.-W. Hammer, and U.-G. Meißner, Phys. Rev. A **70** 052101 (2004).
- [9] E. Braaten and H.-W. Hammer, Phys. Rep. **428**, 259 (2006).
- [10] D. Blume, B. D. Esry, C. H. Greene, N. N. Klausen, and G. J. Hanna, Phys. Rev. Lett. **89**, 163402 (2002).
- [11] D. V. Fedorov, A. S. Jensen, and K. Riisager, Phys. Rev. C **49**, 201 (1994).
- [12] D. V. Fedorov, A. S. Jensen, and K. Riisager, Phys. Rev. C **50**, 2372 (1994).
- [13] A. S. Jensen, K. Riisager, D. V. Fedorov, and E. Garrido, Rev. Mod. Phys. **76**, 215 (2004).
- [14] M. T. Yamashita, L. Tomio, A. Delfino, and T. Frederico, cond-mat/0602549.
- [15] W. C. Stwalley, Phys. Rev. Lett. **37**, 1628 (1976).
- [16] E. Tiesinga, B. J. Verhaar, and H. T. C. Stoof, Phys. Rev. A **47**, 4114 (1993).
- [17] E. A. Donley, N. R. Claussen, S. T. Thompson, and C. E. Wieman, Nature **417**, 529 (2002).
- [18] C. A. Regal, M. Greiner, and D. S. Jin, Phys. Rev. Lett. **92**, 040403 (2004).
- [19] M. W. Zwierlein, C. A. Stan, C. H. Schunck, S. M. F. Raupach, A. J. Kerman, and W. Ketterle, Phys. Rev. Lett. **92**, 120403 (2004).
- [20] V. Efimov, Phys. Lett. **33B**, 563 (1970).
- [21] T. Kraemer, M. Mark, P. Waldburger, J. G. Danzl, C. Chin, B. Engeser, A. D. Lange, K. Pilch, A. Jaakkola, H.-C. Nägerl, and R. Grimm, Nature **440**, 315 (2006).
- [22] C. Chin, T. Kraemer, M. Mark, J. Herbig, P. Waldburger, H.-C. Nägerl, and R. Grimm, Phys. Rev. Lett. **94**, 123201 (2005).
- [23] T. Köhler, K. Góral, and P. S. Julienne, cond-mat/0601420.
- [24] W. Kołos and L. Wolniewicz, Chem. Phys. Lett. **24**, 457 (1974).
- [25] W. Kołos and J. Rychlewski, J. Mol. Spectr. **143**, 237 (1990).
- [26] M. J. Jamieson, A. Dalgarno, and L. Wolniewicz, Phys. Rev. A **61**, 042705 (2000).
- [27] J. F. Bukta and W. J. Meath, Mol. Phys. **27**, 1235 (1974).
- [28] C. Herring and M. Flicker, Phys. Rev. **134**, A362 (1964).
- [29] Z.-C. Yan, J. F. Babb, A. Dalgarno, and G. W. F. Drake, Phys. Rev. A **54**, 2824 (1996).
- [30] P. Courteille, R. S. Freeland, D. J. Heinzen, F. A. van Abeelen, and B. J. Verhaar, Phys. Rev. Lett. **81**, 69 (1998).
- [31] S. Inouye, M. R. Andrews, J. Stenger, H. J. Miesner, D. M. Stamper-Kurn, and W. Ketterle, Nature **392**, 151 (1998).
- [32] J. P. Burke, Jr., C. H. Greene, and J. L. Bohn, Phys. Rev. Lett. **81**, 3355 (1998).
- [33] R. C. Whitten and F. T. Smith, J. Math. Phys. **9**, 1103 (1968).
- [34] D. Blume, C. H. Greene, and B. D. Esry, J. Chem. Phys. **113**, 2145 (2000).
- [35] B. L. Hammond, W. A. Lester, Jr., and P. J. Reynolds, *Monte Carlo Methods in Ab Initio Quantum Chemistry* (World Scientific, Singapore, 1994).
- [36] D. Blume, M. Lewerenz, F. Huisken, and M. Kaloudis, J. Chem. Phys. **105**, 8666 (1996).
- [37] M. Lewerenz, J. Chem. Phys. **106**, 4596 (1997).
- [38] M. V. Rama Krishna, and K. B. Whaley, J. Chem. Phys. **93**, 6738 (1990).
- [39] P. A. Whitlock, D. M. Ceperley, G. V. Chester, and M. H. Kalos, Phys. Rev. B **19**, 5598 (1979).
- [40] D. Blume and C. H. Greene, J. Chem. Phys. **112**, 8053 (2000).
- [41] J. M. Blatt and V. F. Weisskopf, *Theoretical Nuclear Physics* (Wiley, New York, 1952).
- [42] R. G. Newton, *Scattering Theory of Waves and Particles*, Second Edition, Dover Publications, Inc. (2002).
- [43] R. Brühl, A. Kalinin, O. Kornilov, J. P. Toennies, G. C. Hegerfeldt, and M. Stoll, Phys. Rev. Lett. **95**, 063002 (2005).
- [44] B. D. Esry, C. H. Greene, and H. Suno, Phys. Rev. A **65**, 010705(R), (2001).
- [45] R. D. Eppers, J. V. Dugan, Jr., and R. W. Palmer, J. Chem. Phys. **62**, 313 (1975).
- [46] P. F. Bedaque, H.-W. Hammer, and U. van Kolck, Phys. Rev. Lett. **82**, 463 (1999).
- [47] P. F. Bedaque, H.-W. Hammer, and U. van Kolck, Nucl. Phys. A **646**, 444 (1999).
- [48] S. K. Adhikari, T. Frederico, and I. D. Goldman, Phys. Rev. Lett. **74**, 487 (1995).
- [49] S. Nakaichi, Y. Akaishi, H. Tanaka, and T. K. Lim, Phys. Lett. **68A**, 36 (1978).
- [50] S. Nakaichi, T. K. Lim, Y. Akaishi, and H. Tanaka, J. Chem. Phys. **71**, 4430 (1979).
- [51] J. A. Tjon, Phys. Lett. **56B**, 217 (1975).
- [52] J. A. Tjon, Nucl. Phys. **A353**, 47c (1981).
- [53] R. Perne and H. Kröger, Phys. Rev. C **20**, 340 (1979).
- [54] H.-W. Hammer and D. T. Son, Phys. Rev. Lett. **93**, 250408 (2004).
- [55] D. Blume, Phys. Rev. B **72**, 094510 (2005).